J. Phys. France **51** (1990) 103-120 1er JANVIER **1990**, PAGE 103

Classification
Physics Abstracts
61.50J — 61.10 — 68.20

X-ray study of the roughening transition of the Ni(113) surface

I. K. Robinson (1), E. H. Conrad (2) and D. S. Reed (2)

(1) AT & T Bell Laboratories, Murray Hill, New Jersey 07974, U.S.A.
(2) Dept. of Physics & Astronomy, Univ. of Missouri, Columbia MO 65211, U.S.A.

(*Reçu le 9 mai 1989, révisé le 28 août 1989, accepté le 19 septembre 1989*)

Résumé. — Nous présentons des résultats de diffraction X en fonction de la température pour Ni(113) qui montrent des changements spectaculaires des « bâtonnets de terminaison ». La variation de l'intensité est en bon accord avec les travaux antérieurs sur Cu(113) mais nous pouvons maintenant résoudre aussi des changements dans la forme des pics. Nous développons une théorie de la diffraction des surfaces rugueuses et nous l'utilisons pour montrer que la surface a des fluctuations finies d'amplitudes au-dessous de la transition qui deviennent divergentes au-dessus. La forme fonctionnelle de la divergence ne peut cependant pas être évaluée de façon unique.

Abstract. — We present X-ray diffraction data as a function of temperature for Ni(113) that show dramatic changes in one of the crystal truncation rods. The variation of the observed intensity is in good agreement with previous work on Cu(113), but we can now resolve changes of lineshape as well. We develop a theory of diffraction of rough surfaces and use it to show conclusively that the surface has finite height fluctuations below the transition that become divergent above. The exact functional form of the divergence cannot be evaluated uniquely, however.

The stability of a surface can be predicted from its microscopic interactions by the well known Wulff construction [1]. Low-index surfaces are often stable at all temperatures at which the solid exists, but high-index surfaces normally have lower free energy in a rough state whereby the configurational entropy term exceeds the potential energy. An intermediate case however can be smooth at low temperature and rough at high temperature, thereby having a phase transition at the roughening temperature, T_R, first suggested by Burton and Cabrera [2]. This is known to occur in electron microscope studies of the equilibrium crystal shape of small Pb and Cu crystals [3], which present different facets at different temperatures. Recently there have been studies of the stability of extended crystal faces by He and X-ray diffraction that also show a well-defined transition. Agreement with the statistical mechanical theory for $T \ll T_R$ due to Villain *et al.* [4], has been reported in X-ray studies of Cu(110) [5] and Cu(113) [6], while He diffraction work on Ni(115) [7], Ni(113) [8], Cu(115) [9] and X-ray work on Ag(110) [10] have been interpreted in terms of a logarithmic divergence of the height fluctuations valid for $T > T_R$ as originally suggested by Chui and Weeks [11]. We will discuss both these theories in this paper.

Our experiments use X-ray diffraction because the Born approximation ensures that it is accurately kinematical. The diffracted amplitude is just a superposition of scattered contributions from all parts of the sample. Here lies the main advantage over He and electron diffraction which are inherently much more surface sensitive. In this work grazing incident/exit angle conditions were used to reduce background ; a kinematic description of the diffraction is still appropriate however [12]. Surface sensitivity in X-ray diffraction is obtained by using an intense source (synchrotron radiation from an electron storage ring) and selecting, by symmetry only, the parts of the diffraction pattern due to the surface. Because a relatively small total momentum transfer is used, phonon effects are kept to a minimum. The X-ray surface technique has been widely used over the last few years for surface structure determination [13] and recently for studying phase transitions [5, 6, 10, 14].

Before presenting the data for Ni(113) we will write down the theory of X-ray diffraction from rough surfaces and show how it predicts the lineshapes for the two roughening theories mentioned above. This section is based on the theory of crystal truncation rods [15] and is closely analogous to the calculation of He diffraction from rough surfaces [4] with some important differences. It also has some similarity to the calculation of Mochrie [5].

Diffraction from rough surfaces.

We assume a Solid on Solid (SOS) model for the crystal with a rough surface [16] which has all atoms on an ideal cubic lattice truncated by a height function $h(x, y)$ as shown in figure 1a. We use dimensionless crystallographic coordinates such that x and y represent the number of unit cells along the in-plane directions and z is normal to the surface. The components of momentum transfer are similarly dimensionless, (q_x, q_y, q_z). The kinematically scattered amplitude from this arrangement is,

$$A = \sum_{x=1}^{N} \sum_{z=-\infty}^{h(x)} e^{i(q_x x + q_z z)} \tag{1}$$

$$= \sum_{x=1}^{N} e^{i(q_x x + q_z h(x))} \sum_{z'=-\infty}^{0} e^{iq_z z'} . \tag{2}$$

The summation of x implicitly assumes a sum in y as well. The second sum in equation (2) gives rise to the crystal truncation rod in the q_z direction perpendicular to the surface. For mathematical completeness it is necessary to add a small imaginary part to q_z, which attenuates the contributions from deeper layers. This term is then let go to zero [15]. This

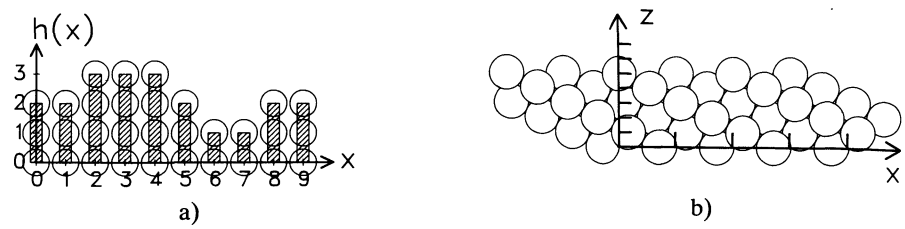

Fig. 1. — (a) The solid on solid (SOS) model of a rough surface of a cubic crystal. The boundary is represented by a single valued function $h(x)$ which is discrete. No overhangs are allowed therefore. (b) Sectional view of a face-centered cubic (f.c.c.) 113 surface. Axes for x and z, respectively parallel and perpendicular to the surface, are marked with ticks representing the distance units of equation (9).

corresponds to the physical situation of absorption of the incident X-ray beam. The result for all points on the rod, except the Bragg points $q_z = 2\pi n$, is [15]

$$A = \sum_{x=1}^{N} e^{i(q_x x + q_z h(x))} \frac{1}{1 - e^{-iq_z}} . \tag{3}$$

The diffracted intensity I is proportional to $\langle AA^* \rangle$ ensemble-averaged over all height configurations

$$I = \frac{1}{2 \sin^2 q_z/2} \left\langle \sum_{xx'} e^{iq_x(x-x')} e^{iq_z(h(x)-h(x'))} \right\rangle . \tag{4}$$

The surface is assumed to be the same everywhere so we can use the stationary property $h(x) - h(x') = h(\xi) - h(0)$ where $\xi = x - x'$.

$$I = \frac{N}{2 \sin^2 q_z/2} \sum_{\xi=1}^{N} e^{iq_x \xi} \langle e^{iq_z(h(\xi)-h(0))} \rangle . \tag{5}$$

The ensemble average in equation (5) is evaluated in reference [4] in terms of the height-height correlation function, which is the quantity predicted by the statistical mechanical models we use. The approximations used [4] are poor for the case of $q_z \simeq (2n + 1)\pi$ which is the case most relevant to this paper, as well as most other experimental work, so we will derive a new expression for the ensemble average in equation (5). We assume that the height of the surface is a *discrete* Gaussian random variable with a distribution

$$P_n = P[(h(\xi) - h(0)) = n] = c\, e^{-\alpha^2 n^2}$$

where α depends on ξ. The ensemble average we require is then

$$\begin{aligned} \langle e^{iq_z(h(\xi)-h(0))} \rangle &= c \sum_n e^{iq_z n - \alpha^2 n^2} \\ &= c \int dx\, e^{iq_z x - \alpha^2 x^2} \sum_n \delta(x - n) \\ &= c \int dx\, e^{iq_z x - \alpha^2 x^2} \sum_p e^{2\pi i p x} \\ &= c \sum_p \left(\frac{\pi}{\alpha^2} \right)^{1/2} e^{-(q_z + 2\pi p)^2/4\alpha^2} . \end{aligned}$$

We will assume that the height distribution is broad so that $\alpha \ll 1$ and the summation in p is dominated by its central term. We can also substitute

$$c = 1 / \sum_n e^{-\alpha^2 n^2} \simeq \left(\frac{\alpha^2}{\pi} \right)^{1/2}$$

$$\langle (h(\xi) - h(0))^2 \rangle = \sum_n n^2 P_n = \frac{1}{2\alpha^2}$$

to obtain

$$\langle e^{iq_z(h(\xi)-h(0))} \rangle = e^{-\langle (h(\xi)-h(0))^2 \rangle [q_z]^2/2}$$

where $[q_z]$ means q_z *modulo* 2π such that $-\pi < [q_z] \leq \pi$. The case of interest $[q_z] \simeq \pi$ will require an extra factor of 2 in the intensity because two terms are equally important in the sum over p, but we will ignore this.

The resulting formula for the intensity is :

$$I = \frac{N}{2 \sin^2 q_z/2} \sum_{\xi} e^{iq_x \xi} e^{-\langle (h(\xi)-h(0))^2 \rangle [q_z]^2/2} . \tag{6}$$

This is the fundamental equation for describing the diffraction of rough surfaces in the SOS model. It contains two factors, an ideal $1/\sin^2 (q_z/2)$ crystal truncation rod [15] (CTR) intensity dependence on the perpendicular momentum transfer q_z, multiplied by the Fourier transform of the pair correlation function $C(\xi)$ parallel to the surface :

$$C(\xi) = e^{-\langle (h(\xi)-h(0))^2 \rangle [q_z]^2/2} . \tag{7}$$

Figure 2 shows some graphic examples of the evaluation of equation (6) for various height autocorrelation functions $\langle (h(\xi) - h(0))^2 \rangle$ shown on the left hand side. The center column shows the correlation function $C(\xi)$ defined in equation (7) and on the right is its Fourier transform, the intensity. Case 2(a) is a rough surface with a linear divergence of $\langle (h(\xi) - h(0))^2 \rangle$ with distance ξ ; it results in a Lorenzian lineshape for the cross section of the truncation rod. The Lorenzian width is proportional to $[q_z]^2$; the rod is therefore sharp close in, but broadens rapidly with $[q_z]$.

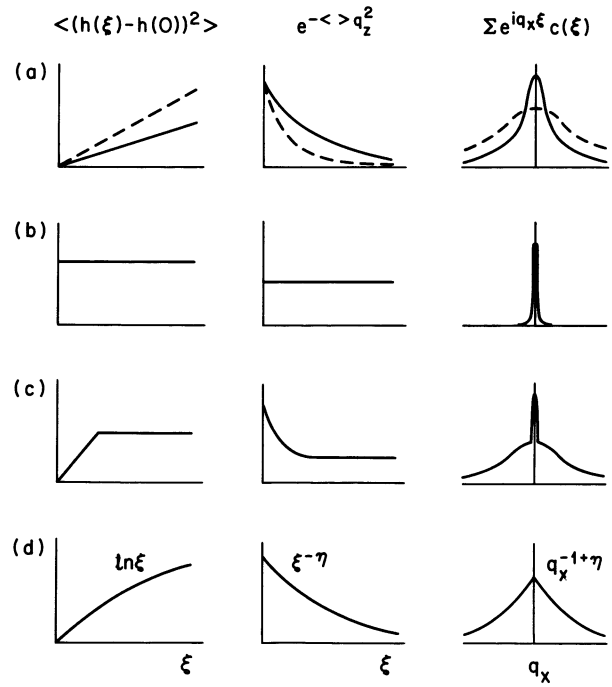

Fig. 2. — One-dimensional calculation of the cross sectional lineshape of a truncation rod from the height-height correlation function. The four cases are in the order discussed in the text. In order of increasing roughness they would be (b), (c), (d), (a).

Case 2(b) is a flat surface, using the definition of having finite height fluctuation at large distance. On any distance scale there is a certain random variation of height specified by its root mean square value h_0. This results in diffraction which is sharp in cross section, as indicated by a δ-function in q_x. However, the intensity varies with q_z according to

$$I \propto \frac{\delta(q_x - 2\pi n)}{\sin^2 q_z/2} e^{-h_0^2[q_z]^2} . \tag{8}$$

This Debye-Waller-like expression is analogous to the description of a « rough » surface given in reference [15] in the sense that the intensity falls away from the Bragg points more steeply than the classical $1/\sin^2(q_z/2)$ crystal truncation rod. The distribution function here is Gaussian instead of exponential, so the functional form of equation (8) is different from that of reference [15]. In the context of roughening transitions we would classify this surface as smooth because the height fluctuations do not diverge. The signature is the presence of the δ-function cross section of the rod.

Case 2(c) is intermediate between (a) and (b) having long range flat asymptotic behaviour and linearly increasing height correlations at short range. This gives rise to both sharp and broad features in the diffraction. The example shown is particularly simple, giving a lineshape which is the sum of a δ-function and a Lorenzian.

The last case 2(d) illustrates the roughness predicted by Chui and Weeks [11] for $T > T_R$ where the height fluctuations diverge logarithmically in ξ. This gives rise to a power law lineshape as shown. This surface is asymptotically rough but less so than case 2(a) and so has a diffraction lineshape which is intermediate between case 2(a) and 2(c). Further discussion of roughness models and their diffraction patterns is deferred to the next section.

Equation (6) is a simple periodic function in q_z because the height function $h(x)$ can only take discrete (integer) values. If we consider the more general case of a crystal with a basis or one cut to any other direction than (100), the function assumes the periodicity of the new reciprocal lattice instead. This is illustrated for the Ni(113) surface in figure 1b. This ideally « flat » configuration of the surface shown is used as the reference xy plane. With respect to the cubic lattice a regular array of terraces and steps is perceived in this plane. Upon roughening, the spacing of the steps becomes irregular with consequential height fluctuations in z. We can use the same crystallographic coordinates for (x, y, z) if the unit cell is defined as shown by the axes of the figure. The definition is orthorhombic ; to convert to physical distance (Å) units $(\tilde{x}, \tilde{y}, \tilde{z})$ defined along the same directions we need :

$$\left.\begin{aligned} \tilde{x} &= \frac{11}{8} a_0 x \\ \tilde{y} &= \frac{1}{\sqrt{2}} a_0 y \\ \tilde{z} &= \frac{1}{\sqrt{11}} a_0 z \end{aligned}\right\} \tag{9}$$

where a_0 is the f.c.c. lattice parameter, 3.524 Å for Ni. The reciprocal of transformation (9) relates $(q_x q_y q_z)$ to $(\tilde{q}_x \tilde{q}_y \tilde{q}_z)$ in physical (Å^{-1}) units.

The reciprocal lattice is shown in figure 3. Crystal truncation rods (CTR) emanate from each bulk Bragg point in the direction of the surface normal, which is 113 here. This has the consequence of linking the 002 reflection to $\overline{111}$ on the first-order rod as shown. Since q_z is now defined by equation (9) in units of the reciprocal layer spacing, equation (6) can be used in its existing form with a suitable shift of origin so that $[q_z]$ and sin $(q_z/2)$ are zero at

every Bragg point. This recentering means that measurements can be made with momentum transfer parallel to the surface (as in the advantageous grazing incidence/grazing exit angle geometry), yet still permitting large values of $[q_z]$ to be attained.

All measurements presented here were made on the first-order CTR of Ni(113) at its point of intersection with the surface plane $(\overline{664})/11$. The incidence and exit angles were both approximately equal to the critical angle for total external reflection, optimally suppressing background from the bulk and enhancing the signal by refraction [12, 13]. The nearest Bragg peak is seen in figure 3 to be $(\overline{111})$ which is a reciprocal space distance $[q_z] = 2\,\pi\,\frac{5}{11}$ away. It is therefore close to the antinode, $[q_z] = \pi$, midway between two Bragg peaks (the « anti Bragg » position referred to in He scattering), that gives the maximum sensitivity to roughness, as can be seen directly in equation (6).

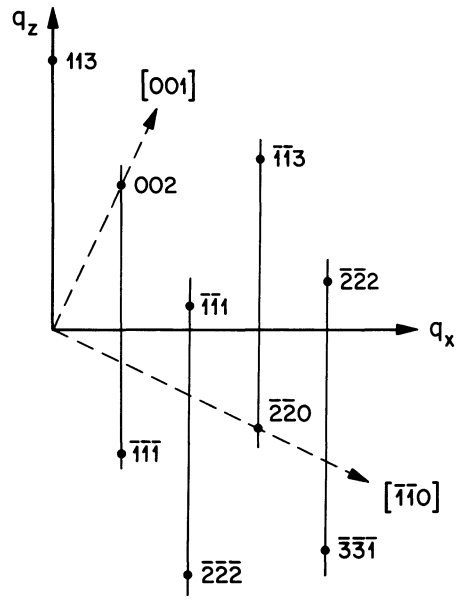

Fig. 3. — Reciprocal space diagram for the 113 cut through a face centered cubic lattice. Dots representing Bragg peaks are indexed traditionally. q_x and q_z are respectively parallel and perpendicular to the surface as used in the text. Crystal truncation rods (CTRs) link Bragg peaks together in the perpendicular direction. The intensity of the rod depends on the state of roughness of the surface and has a functional form in $(q_x\,q_z)$ predicted by equation (6).

A sensitive test of the theory presented above is its q_z dependence. For example, the width of the lineshape in q_x should be quadratic in the distance to the nearest Bragg point, as should the value of the exponent η appearing in figure 2d and discussed below. It is important to test this behaviour because large scale variations in the direction of the surface normal will also change the widths of the rods, but in a way that is linear in $[q_z]$. For the 113 surface (Fig. 3) the q_z dependence is readily tested because the distance of the intersection of the *second* order CTR with the surface plane is only a distance $[q_z] = 2\,\pi/11$ from the $(\overline{111})$ Bragg peak. Unfortunately, although the rod was easily detected here, reliable measurements as a function of temperature were not obtained here for our sample.

Roughening model for $T \leqslant T_R$.

Here we consider the terrace-step-kink (TSK) model of Villain *et al.* [4] for the low temperature behaviour of a surface with a well defined « flat » state described by a step-and-terrace picture of figure 1b. The elementary excitation that leads to roughening is a pair of kinks separated by a run of n displaced step edges. The density of such excitations in the $T \ll T_R$ limit is sufficiently low that they do not interact significantly. The energy of the local excitation is

$$E_n = 2\,W_0 + n\omega \tag{10}$$

where W_0 is the kink energy and ω is the energy per site to displace a step. The height of the surface is increased or decreased by one vertical lattice spacing over the n sites that are displaced. The mean square height is evaluated assuming a Boltzman distribution and $W_0 \gg kT_R \gg \omega$

$$\langle h^2 \rangle = \frac{\sum_{n=1}^{\infty} 2\,n\,e^{-E_n/kT}}{1 + 2\sum_{n=0}^{\infty} e^{-E_n/kT}} = 2(kT/\omega)^2\,e^{-2W_0/kT}\,. \tag{11}$$

Because no interactions are assumed there are no correlations in the height distribution which is therefore independent of ξ. $2\langle h^2 \rangle$ can be substituted for $\langle (h(\xi) - h(0))^2 \rangle$ in equation (8) which leads to a δ-function lineshape with an intensity

$$I \propto \frac{\delta(q_x - 2\pi n)}{\sin^2 q_z/2}\, e^{-2(kT/\omega)^2 e^{-2(W_0/kT)}[q_z]^2}. \tag{12}$$

This was the functional form used to analyze X-ray data for Cu(110) [5] and Cu(113) [6]. In each case the integrated intensity was used since no change in lineshape was detected. The quoted values of W_0/ω were 2260/170 K and 2100/65 K for Cu(110) [5] and Cu(113) [6] respectively. The values of ω have been adjusted for consistency with the definitions in equation (12).

Roughening models for $T \geqslant T_R$.

We will consider here the results of different theoretical analyses that can be applied to the f.c.c. (113) surface at and above its roughening temperature, T_R. We have redefined the length scales for consistency with the definition of figure 1b and equation (9).

We start with the simple cubic SOS model of figure 1a. A harmonic Hamiltonian is used to describe the energy of interaction between columns summing over nearest neighbours ij

$$E = J \sum_{ij} (h(x_i) - h(x_j))^2\,. \tag{13}$$

This disfavours double height steps between columns. Chui and Weeks have shown [11] that the SOS model gives rise to a roughening transition and that the height-height correlation function diverges logarithmically with distance along the surface. We will use a general expression for this behaviour to include possible anisotropy between the x and y directions.

$$\langle (h(\xi) - h(0))^2 \rangle = X \ln\,[c_x^2\,\xi_x^2 + c_y^2\,\xi_y^2]\,, \tag{14}$$

where the dimensionless coefficients are in general temperature-dependent. $c_x = c_y = 1$ for the simple cubic SOS model.

The Body-Centered Solid-on-Solid (BCSOS) model [16] is a more appropriate extension of this model to the (001) faces of fcc metals. This model includes a sublattice of vertical columns at (1/2, 1/2, 1/2) times the conventional lattice vectors. This model has also been shown to exhibit a roughening transition [17].

The extension of this model to the (113) surface is accomplished by applying the correct periodic boundary in the parallel direction. Kinks at step edges are the major excitation in this model since a kink, unlike a vacancy on the (001) terrace, has fewer nearest neighbor columns with different heights. Interactions between steps are not specifically included in this model. However, a short range repulsion is implied, because equation (13) excludes a significant density of double step heights on the surface. Thus, this effective interaction inhibits step collapse. It is worth noting that the BCSOS model does not limit whether a kink is more than one atomic row deep, so that steps are allowed to advance by more than a single row of atoms. The height-height correlation function has been calculated by Den Nijs *et al.* [18] to have the same logarithmic form of equation (14) for $T > T_R$ with :

$$c_x = c_y = \frac{1}{2} \tag{15a}$$

$$X(T = T_R) = \frac{1}{\pi^2}. \tag{15b}$$

However, the lack of an explicit step-step interaction in the BCSOS model means there is no prediction of the temperature dependence of X.

Another model for $T > T_R$ is discussed by Villain *et al.* [4], deriving its Hamiltonian from Jose *et al.* [19], expressed in the language of kinks in the steps (see previous section) instead of column heights. The columns of this model are in effect aligned with the terraces instead of vertical. We will also refer to it as a terrace-step-kink (TSK) model. Explicit step-step interactions are included. The Hamiltonian is shown to reduce to a form similar to equation (13) that retains the anisotropy between W_0 and ω when these are removed [4]. The TSK model again gives the logarithmic form for the height-height correlation function above T_R with predicted coefficients [4].

$$c_x = \frac{1}{c_y} = \left(\frac{kT}{2\omega} e^{W_0/kT} \right)^{1/2} \tag{16a}$$

$$X(T \geqslant T_R) = \frac{1}{\pi} \left(\frac{kT}{2\omega} e^{-W_0/kT} \right)^{1/2} \tag{16b}$$

where ω and W_0 are the energies defined in the previous section, satisfying $\omega \ll kT \ll W_0$. The model is shown to have a Kosterlitz-Thouless transition at the roughening temperature which itself satisfies

$$\omega = \frac{\pi^2}{2} kT_R e^{-W_0/kT_R} \tag{17}$$

from which the value of X at $T = T_R$ is seen to be the same as for the BCSOS model

$$X(T = T_R) = \frac{1}{\pi^2}. \tag{18}$$

We can calculate the diffracted intensity by inserting equation (14) directly into

equation (6). The logarithmic dependence on distance gives rise to a powerlaw correlation function :

$$C(\xi) = [c_x^2 \xi_x^2 + c_y^2 \xi_y^2]^{-X[q_z]^2/2} \tag{19}$$

from which the intensity is calculated by Fourier transformation

$$I = \frac{N}{2 \sin^2 q_z/2} \frac{\Gamma(2-\eta)}{\Gamma\left(\frac{\eta}{2}\right)\Gamma\left(\frac{3}{2}-\frac{\eta}{2}\right)} \left[\frac{[q_x]^2}{c_x^2} + \frac{[q_y]^2}{c_y^2}\right]^{\frac{\eta}{2}-1} \tag{20}$$

where $[q_x]$ and $[q_y]$ are also *modulo* 2π, being the momentum transfer deviations from the nearest Bragg rod. The exponent, η, has the temperature dependence of the coefficient X

$$\eta = X(T)\,[q_z]^2\,. \tag{21}$$

At the Bragg peaks, $\sin(q_z/2) = 0$ and $\eta = 0$. Equation (20) then degenerates to the expected δ-function form in q_x q_y and q_z. From equation (18) or (15b) it readily seen that the value of the exponent at the most sensitive diffraction position $q_z = \pi$ at the roughening transition is $\eta = 1$.

Experimental methods.

X-ray measurements were made on beam line X16A at the National Synchrotron Light Source (NSLS) at Brookhaven National Lab. 5 milliradians of radiation were focussed by a toroidal Pt-coated mirror at 5.67 milliradians incident angle. Two parallel Si(111) crystals selected the wavelength of 1.5 Å, chosen to lie below the Ni adsorption edge. The sample sat at the focus of the beam, at the center of a 4-circle diffractometer and in a pressure of 2×10^{-10} Torr maintained by ion pumps and a Ti sublimator. The design of our Ultra High Vacuum (UHV) diffractometer is published elsewhere [20]. Resolution was determined by the mirror for the incident beam and by 2 mm slits at 500 mm for the exit beam. The former was < 0.001 Å^{-1} and so was unimportant ; the latter determined the instrumental resolution of 0.0149 Å^{-1} radial and 0.0053 Å^{-1} transverse at the first-order CTR position.

The sample was cut from a single crystal by spark erosion. The face was cut slightly convex so that the exact 113 direction could be selected by suitable translation. In fact this translation served a second purpose of allowing us to search for a large flat region on the surface, which was probably more important. The surface was first prepared by electrochemical etching in 50 % H_2SO_4 at 0.5 A cm^{-2}, then by heating in O_2, then by sputtering and annealing. Contamination of the surface by S was found not to be a problem below 1 150 K ; carbon contamination occurred slowly during each experiment but was never more than 1 %. The sample was heated radiatively and the temperature was measured with a chromel/alumel thermocouple, calibrated using the thermal expansion coefficient of 1.35×10^{-5} K^{-1}.

The sample was aligned using the out-of-plane $\bar{3}11$ and $1\bar{3}1$ bulk Bragg peaks at 670 K to determine an orientation matrix ; thermal offsets at the roughening temperature were thereby reduced. Scans were made through the first-order CTR in the q_x radial [parallel to $(\bar{3}\bar{3}2)$] and q_y transverse [parallel to $(\bar{1}10)$] directions extending far enough to establish a clear background. The point on the rod was slightly above $\bar{6}/11$ $\bar{6}/11$ 4/11 in order to achieve grazing incidence. Examples of q_x scans are shown in figure 4.

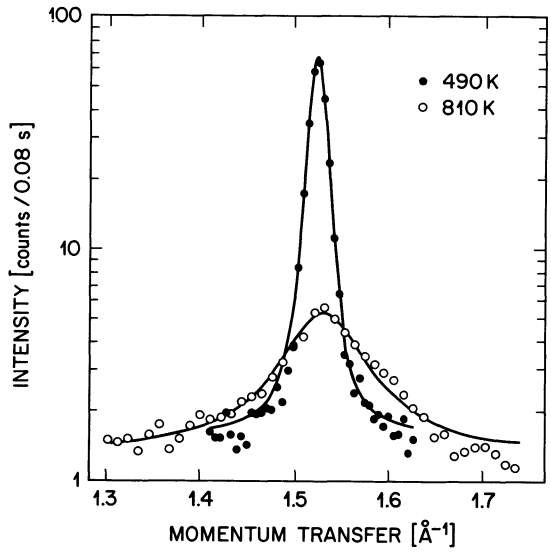

Fig. 4. — Lineshapes measured at $\bar{6}/11\ \bar{6}/11\ 4/11$ with radial scans (along $\tilde{q}_x$ at temperatures above and below T_R. The fitting curves are Lorenzians convoluted with the Gaussian instrumental resolution. These 2D L * G fits were performed simultaneously in $\tilde{q}_x$ and $\tilde{q}_y$.

Result and discussion $T < T_R$.

The temperature dependence is immediately evident in the radial lineshape shown in figure 4 : the intensity drops dramatically in the center of the scan and rises in the adjacent regions as temperature is raised. The same behaviour is seen in the transverse q_y direction. The central part of the low temperature lineshape is resolution limited in both directions.

A simple lineshape that fits simultaneously the radial and transverse data at all temperatures is a simple Lorenzian, convoluted with the known resolution parameters, assuming this to be Gaussian. We denote these L * G fits. Goodness of fit was established by the conventional χ^2 considering only counting statistics as the source of experimental error. For these fits a height, two widths, two peak positions and a background were the parameters and the result was a χ^2 of 2.7 averaged over all temperatures, will the worst case $\chi^2 = 3.6$.

Figure 5a shows the dependence of peak height with temperature. It follows roughly the same TSK curve from the Villain theory [4] (Eq. (12)) that explained the Cu(113) data [6] with a roughening temperature ~ 150 K higher. However closer inspection shows this curve to be inadequate at the high T end : the full and dashed TSK curves shown have values of W_0/ω of 4 300 K/10 K and 2 700 K/100 K which are both at the limits of acceptability for $T < 720$ K. Above 720 K the agreement is bad. From equation (17) we conclude that $T_R = 740 \pm 20$ K, assuming the two cases shown to be the extrema of the fit. $W_0 = 4\,000$ K is already of the order of the estimate of the energy of the Ni-Ni bond that would be broken to form the kink if there were no relaxation [4], so higher values would be considered unreasonable.

Note that Debye-Waller corrections have not been included in the analysis simply because of the small momentum transfers used in these experiments, $|Q| = 1.5$ Å^{-1}. These corrections would multiply equation (12) by a term e^{-2M}. Using previous reported values for $2M$, including anharmonic terms, for bulk Ni gives $2M = 0.04$ at 900 K under the scattering

conditions in these experiments [21]. Values from He scattering measurements on Ni(113) would similarly give $2M = 0.06$ [22]. The exponent in equation (12) used to fit the data in figure 5, however, ranges between 3.3 to 9.4 so that Debye-Waller correction to the fits are negligible. Corrections to W_0 and ω from inelastic scattering are much less than 1 % and can be ignored. The low value of $2M$ has important consequences in the analysis of diffraction line shapes as discussed in the next section.

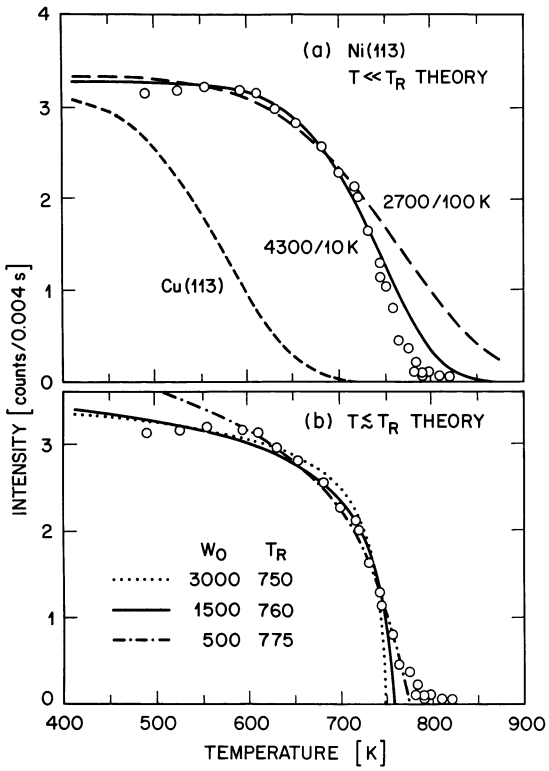

Fig. 5. — Temperature dependence of the peak height of the first order CTR at $\bar{6}/11\ \bar{6}/11\ 4/11$ obtained by means of L * G fits. (a) Theoretical curves are from the $T \ll T_R$ limit of the TSK model (Eq. (12) and Ref. [4]) with parameter values W_0/ω indicated. The dashed curve marked Cu(113) is the best fit to the behaviour of that surface measured by Liang *et al.* (Ref. [6]) with $W_0 = 2\,100$ K $\omega = 65$ K. (b) Theoretical curves for the $T \lesssim T_R$ renormalization group expansion of the TSK model (Eq. (24) and Ref. [4]), with parameter values W_0 and T_R indicated.

The explanation we favour for the disagreement in figure 5a is that we are seeing the breakdown of the Villain $T \ll T_R$ theory in the vicinity of T_R. This means the values of W_0 and ω obtained here and in previous work should have much larger error bars than claimed [6], as figure 5 demonstrates. However, it is still hard to account for the discrepancy in these fitted values with He scattering values for W_0 and ω [23]. The breakdown of the TSK $T \ll T_R$ theory is not a surprise when $T \sim T_R$ because the density of kinks is so high they can no longer be considered isolated and non-interacting.

Villain *et al.* [4] have in fact derived another expression for the height correlation function for $T < T_R$ that applies close to the roughening temperature. This comes from the

renormalization description of the TSK model mentioned above, that predicts Kosterlitz-Thouless behaviour at the transition :

$$\langle (h(\xi) - h(0))^2 \rangle = \frac{2}{\pi^2} \left[\alpha^{-1/2} \left(\frac{T_R - T}{T_R} \right)^{-1/2} - K(\xi) \right] \tag{22}$$

where $K(\xi)$ decays exponentially at large ξ and α is a constant that depends on W_0,

$$\alpha = \frac{8 \pi W_0}{\sqrt{5}\, k T_R}. \tag{23}$$

Neglecting the finite-range ξ-dependent term which gives rise to a broad component in the diffraction, as it does in figure 2c, we can substitute equation (22) into equation (8) to obtain the temperature dependence of the sharp, Bragg component :

$$I \propto \frac{\delta (q_x - 2 \pi n)}{\sin^2 q_z/2} \, e^{-\alpha^{-1/2} \left(\frac{T_R - T}{T_R} \right)^{-1/2} [q_z]^2/\pi^2}. \tag{24}$$

Figure 5b shows fits to equation (24) for different values of W_0 and T_R. The best overall fit is with $W_0 = 1\,500$ K, $T_R = 760$ K ; values of W_0 above 3 000 K are ruled out, even though it is rather insensitive to this parameter.

Between the two limiting cases of the TSK theory, equation (12) and equation (24), we therefore cover the whole range up to T_R using more or less the same parameter values. The non-interacting kink approximation works for $T \ll T_R$ while the renormalization group expansion works for $T \lesssim T_R$ as expected. The tailing of the data just above T_R could not be explained in the TSK model, but can be understood with the KT description as either the height of the diffuse component above T_R or inhomogeneous broadening of the transition due to strain gradients in the sample.

The appearance of a broad component starting just below T_R is confirmed in figure 6 by the T dependence of the Lorenz widths from the same fits. The widths are constant until a threshold value is reached near $T = 740$ K, and diverge above. The threshold is not sharp as it is for other surface phase transitions [14], so it is not possible to determine an accurate transition temperature in this way. The difference between the widths in the transverse and radial direction is a measure of the surface anisotropy defined in equations (14) and (16a) which is discussed below.

Results and discussion $T > T_R$.

To check for consistency with the prediction of logarithmic divergence of the height-height correlation function for $T > T_R$ and to investigate the uniqueness of the fitting methods, we have also fit the diffraction profiles in two further ways. First, a one dimensional convolution of equation (20) was made with the Gaussian instrument response function. The resolution function, which includes finite size effects, was determined from the bulk peak profiles as before. The adjustable parameters in the power-law fits were the exponent η, the peak height, and background. The quality of the power-law fits was compared with the L * G fits over the entire experimental temperature range. Below 750 K the χ^2 values of L * G were about a factor of 2 lower than the power law fits. Above 750 K both fitting procedures produced roughly equal fits with typical $\chi^2 \sim 2.5$. An example of the convoluted power law fits is shown in figure 7.

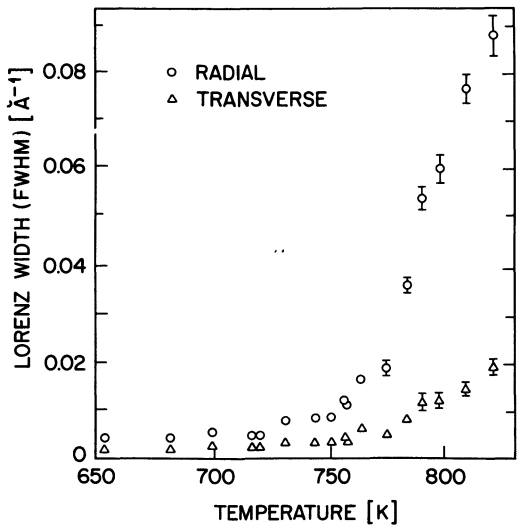

Fig. 6. — Temperature dependence of the radial ($\tilde{q}_x$) and transverse ($\tilde{q}_y$) Lorenzians widths obtained from two dimensional L * G fits including those shown in figure 4.

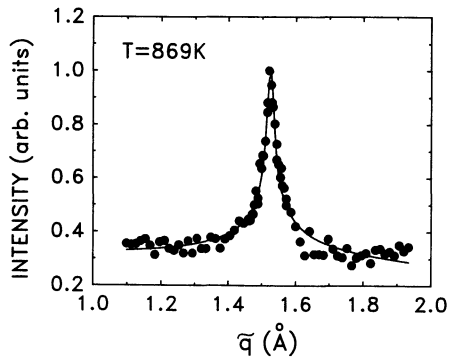

Fig. 7. — Typical radial scan across the CTR connecting the (002) and ($\bar{1}1\bar{1}$) bulk reflections. The intensity is plotted as a function of the momentum transfer $\tilde{q}_x$. The scan was taken at a value of $[q_z] = 0.91\ \pi$, close to the out-of-phase condition. The solid line is a fit to the data using the power law form of equation (17) convoluted with the finite crystal size as explained in the text.

While η is strictly zero below T_R, fitting the data to a power law peak shape over the entire temperature range is instructive for two reasons. First, it allows a view, by comparison with the L * G fits, of the evolution of the lineshape through the transition. Second, the value of η below T_R is a measure of both the one-phonon broadening and any residual defect broadening of the low temperature peak shapes [9, 22]. The latter point is particularly useful in judging the accuracy of the lineshape fits due to corrections from these effects.

A second and more intuitive method to obtain the exponent η is to plot the data logarithmically as in figure 8. From equation (17), the slope of the log-log plots is proportional to η. The advantage of this method is that data points near the peak, which are strongly influenced by the detector response and crystal perfection, can be identified and

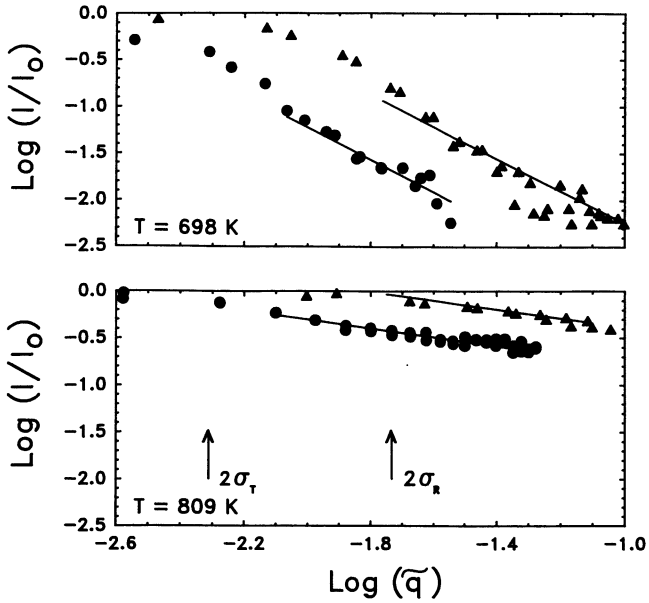

Fig. 8. — Log(I) *versus* log($\tilde{q}$) for radial q_x(△) and transverse q_y(●) directions taken at temperatures above and below T_R. At a given temperature the linear region of the log-log plots for both radial and transverse directions have the same slope of η-2. The asymmetry between $\tilde{q}_x$ and $\tilde{q}_y$ is clearly evident as a horizontal shift.

ignored : all of the fits excluded data less than 2 σ away from the central peak. This means that η was determined over a range of correlation lengths between 1 300 Å to 100 Å, probing ten times further than previous studies [7-9]. The values of η determined by the power law peak profiles and those measured from the log-log plots agreed with each other within the error bars of the χ^2 fitting routines. This justifies our claim that instrumental and finite-size effects are unimportant in the full lineshape fits.

At each temperature the values of η determined separately from the radial and transverse scans were found to be essentially the same, as figure 9 shows. Using equation (21), the roughening temperature was determined from the temperature at which $X(T) = 1/\pi^2$: using the value of 10 $\pi/11$ for q_z, η should have a value of 0.83 at T_R. From figure 9 this gives a roughening temperature of 770 K ± 30 K. This value is in good agreement with that obtained in previous atom scattering studies of Ni(113) analyzed by the same method [8]. It also agrees with the value in the previous section for the intensity dependence at $T < T_R$.

The temperature dependence of η is also predicted for the TSK model through equations (16) and (21). Drawn in figure 9 are two curves with different values of the TSK parameters. The curve corresponding to the $T \ll T_R$ parameters of figure 5 gives too small a slope for $\eta(T)$ near $T = T_R$ to explain the data. It is necessary to increase W_0 to 10^4 K in order to get a good fit ; this value is totally unphysical however [4]. Our data are significantly different from the atom scattering measurements for Ni(113) [8, 17], Cu(113) [23] and Cu(115) [9, 24] which find $\eta \propto T$ over a wide range of T and see only a small change in slope of η *vs.* T near T_R. The reason for this is the much smaller one-phonon braodening in the X-ray experiments. In atom scattering experiments, the total momentum transfers are large, typically 5.9 Å^{-1} [7-9, 24], and the $\eta(T)$ curve is significantly affected by the way the fitting is corrected for inelastic effects : a comparison between figure 1 of reference [25] and figure 3

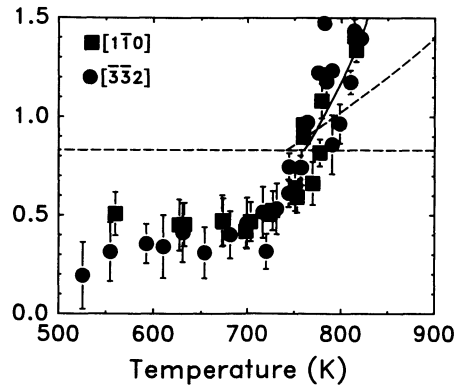

Fig. 9. — Plot of the exponent, η, *versus* temperature. Data for both q_x and q_y directions are included. The roughening temperature is determined to be 770 ± 30 K from the temperature at which $X(T)$ equals $1/\pi^2$, hence $\eta = 0.83$. The dashed curve in from equations (16b) and (21) corresponding to the TSK model with $W_0 = 3\,500$ K $\omega = 32$ K that was used in figure 5. The full curve has $W_0 = 10^4$ K $\omega = 0.007$ K.

of reference [18] shows this clearly. In our X-ray measurements, with a total momentum transfer of 1.5 Å^{-1}, the number of one-phonon scattering events (those primarily responsible for distortions of the lineshape), proportional to $|Q|^2$ [26], is ten times smaller. Inelastic scattering probably does account for the non-zero effective value of $\eta \sim 0.4$ seen for $T \ll T_R$. The TSK theory predicts $\eta = 0$, whereas pure one-phonon inelastic scattering would give a lineshape with $\eta = 1$. *Without correction* the atom scattering experiments gave values of $\eta \sim 0.6$ to 0.8 [7-9, 24] for $T \ll T_R$. We therefore expect our determination of η to be more reliable.

Because both the TSK and BCSOS models for the roughening transition presented so far predict a power-law lineshape for $T > T_R$, a more critical test, which differentiates between the theories, is to examine the lineshape asymmetry, which is directly related to the surface tension anisotropy. X-ray scattering is a particularly important technique here because of its high resolution.

The peak asymmetry is characterizd by the parameter c_x/c_y in equations (14) and (20), which, for the TSK model as equation (16a) indicates, is a relative measure of the ratio of the kink energy, W_0, to the step-step interaction energy, ω. We have measured this parameter in three ways. First, a full 2D convolution of the instrument (plus finite size effects) with the power-law form of equations (17), and (18) was performed. The second method uses the observation that, if the radial and transverse scans are plotted on the same logarithmic scale (Fig. 8), the asymmetry is the displacement in q between the curves. As in the determination of the exponent η, this method reduces errors associated with the detector convolution. These two methods gave the same values of c_x/c_y within error. The third method is to take the ratio of the widths of the L * G fits from figure 6. This gave slightly different results. We have retained the normalized system of $(q_x\, q_y)$ units of figure 1b. In natural $(\tilde{q}_x\, \tilde{q}_y)$ units the asymmetry is $\sqrt{11/4}$ times less pronounced according to equation (9). The results are plotted in figure 10.

In these experiments c_x/c_y is found to increase with temperature. From equation (16a) the TSK model predicts a decrease with temperature above T_R since $kT \ll W_0$. Atom scattering experiments found values that were constant over a wide range of temperature ; the asymmetry c_x/c_y was 1.25 for Ni(113) [8], 2.0 for Cu(113) [23] and 5.0 for Cu(115) [24].

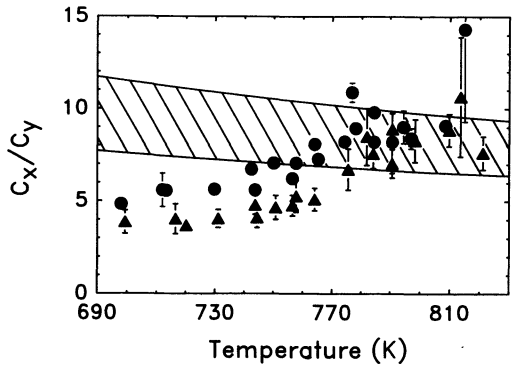

Fig. 10. — The lineshape asymmetry c_x/c_y as a function of temperature. This reflects the anisotropy of the surface tension. Fits to the data of both powerlaw (•) and L * G (△) lineshapes were used and differ slightly. The theoretical curves refer to the TSK model discussed in the text. The range of parameters shaded for the TSK model is $2\,300 < W_0 < 2\,600$ K constrained so that $T_R = 740$ K by equation (17).

Although we find large discrepancies for $T < T_R$ where the theory is not valid anyway, the region $T > T_R$ shows a relatively flat temperature dependence that can be considered consistent with theory. The numerical value of c_x/c_y here of 8.5 ± 1 requires $W_0 = 2\,450$ K $\pm$ 150 K when T_R is fixed at 740 K (not critical) as shown. The value of $W_0 = 3\,500$ K found for $T \ll T_R$ (Fig. 5) would predict $c_x/c_y = 34$.

The BCSOS model (Eq. (15a)) predicts $c_x/c_y = 1$ which is clearly invalid. The asymmetry we observe lies between the predictions for the two models. We can suggest therefore that an intermediate model, for example the anisotropic BCSOS model in which the anisotropy is adjustable [16], might be better.

Summary and conclusions.

We have presented a theory which shows how X-ray diffraction profiles of crystal truncation rods (CTR) can be interpreted in terms of statistical-mechanical models of roughening. We used this to analyse data for the 1st order CTR of Ni(113) as a function of temperature. A simple Lorenzian lineshape was found to be indistinguishable from the expected power-law lineshape in the range $T > T_R$, but gave a better fit for $T < T_R$. This lack of sensitivity shows that the data are still inadequately accurate to *prove* the correctness of the logarithmic divergence of height with distance at $T > T_R$ predicted by Chui and Weeks [11], although they are certainly consistent.

Below T_R we find the lineshape to be a resolution-limited 2D Bragg peak, whose intensity dependence (Fig. 5) on T for $T \ll T_R$ is consistent with the non-interacting kink theory of Villain *et al.* [4]. From this we obtain the microscopic parameters of the TSK model : $W_0 = 3\,500 \pm 800$ K, $\omega = 55 \pm 45$ K consistent with a value of the roughening temperature $T_R = 740 \pm 20$ K. We see significant deviation from the theory as T approaches T_R, and much better agreement with the renormalization group analysis of the same model [4]. Consistency with the prediction of Kosterlitz-Thouless behaviour near T_R is observed with reasonable parameter values $500\text{ K} < W_0 < 3\,000$ K and $T_R = 760 \pm 10$ K.

Above T_R we find significant disagreement with the TSK model. Firstly, for any reasonable values of the microscopic parameters, our experiment shows a much steeper temperature dependence (Fig. 9) of the lineshape exponent η near T_R than predicted. This steep slope also disagrees with the atom scattering data, which is more strongly affected by inelastic

contributions to the lineshape. The determination of $T_R = 770 \pm 30$ K from the crossing of $\eta(T)$ through unity appears to be reliable and consistent with the $T < T_R$ result. Secondly, we measure a lineshape anisotropy (Fig. 10) of $c_x/c_y = 8.5 \pm 1$ for $T > T_R$, compared with 1.25 for Ni(113) [8], 2.0 for Cu(113) [23] and 5.0 for Cu(115) [24] measured with atom scattering, and compared with 34 required from the TSK theory with the above parameter values. Lowering W_0 to $2\,450 \pm 150$ K is needed for consistency here (Eq. (16a)). The alternative BCSOS model [18] predicts no anisotropy and so can be ruled out, although anisotropic versions [16] could be viable.

We note in closing that the $T < T_R$ and $T > T_R$ TSK parameters are about an error-bar apart. The various parameter determinations are listed in table I. A consensus set of parameters marginally consistent with all data (except $\eta(T)$) would be $W_0 = 2\,650 \pm 300$ K, $\omega = 110 \pm 80$ K giving $T_R = 755 \pm 15$ K. This would appear to scale well with the X-ray results for Cu(113) [6] [$W_0 = 2\,100$ K $\omega = 65$ K], but not with the atom-scattering values for Ni(113) [8] [$W_0 = 1\,700 \pm 500$ K, $\omega = 200 \pm 100$ K] or for Cu(113) [23] [$W_0 = 800 \pm 80$ K, $\omega = 560 \pm 60$ K], although this may be because of different analysis techniques. The main new finding of this work is the large value of the anisotropy c_x/c_y above T_R. This is directly apparent from the raw linewidth data (Fig. 6), but also clearly seen in the lineshape analysis.

Table I. — *Summary of fit parameters for the* TSK *model* (Ref. [4]) *derived from different analyses of the X-ray data. Measured values (in* Kelvin*) are stated, while those derived from equation* (17) *are in parentheses. Theory* A *refers to the non-interacting kink approximation* (*Eqs.* (10-12) *and Ref.* [4]) ; *theory* B *refers to the renormalization group treatment of reference* [4].

T	Data	Theory	Figure	Equation	W_0	ω	T_R
—	—	—	—	—	—	—	—
$\ll T_R$	Intensity *vs.* T	A	5(a)	(12)	$3\,500 \pm 800$	55 ± 45	$[740 \pm 20]$
$\lesssim T_R$	Intensity *vs.* T	B	5(b)	(24)	$1\,700 \pm 1\,200$	[400]	760 ± 10
$\gtrsim T_R$	η *vs.* T	B	9	(16b, 18)	10^4	—	770 ± 30
$> T_R$	Anisotropy	B	10	(16a)	$2\,450 \pm 150$	$[150 \pm 30]$	—
	Consensus				2 650	110	755

Acknowledgements.

We wish to thank J. D. Axe, J. Bohr and S. G. J. Mochrie for helpful discussion on the theory of diffraction from rough surfaces and V. Straughan of Monocrystals Inc. for cutting the crystal. NSLS is supported by DOE Grant No. DE-AC012-76CH00016. Work at U. of Missouri was supported by the NSF under Grant No. DMR8703750 and the U. of Missouri Faculty Development Fund.

References

[1] ZANGWILL A., Physics at Surfaces (Cambridge U. Press) 1987.
[2] BURTON W. K., CABRERA N., *Disc. Faraday Soc.* **5** (1949) 33.
[3] HEYRAUD J. C., MÉTOIS J. J., *Surf. Sci.* **128** (1983) 334.
[4] VILLAIN J., GREMPEL D. R., LAPUJOULADE J., *J. Phys. F.* **15** (1985) 809.
[5] MOCHRIE S. G. J., *Phys. Rev. Lett.* **59** (1987) 304.

[6] LIANG K. S., SIROTA E. B., D'AMICO K. L., HUGHES G. J., SINHA S. K., *Phys. Rev. Lett.* **59** (1987) 2447.
[7] CONRAD E. H., ATEN R. M., KAUFMAN D. S., ALLEN L. R., ENGEL T., DEN NIJS M., RIEDEL E. K., *J. Chem. Phys.* **84** (1986) 1015.
[8] CONRAD E. H., ALLEN L. R., BLANCHARD D. L., ENGEL T., *Surf. Sci.* **187** (1987) 265.
[9] FABRE F., GORSE D., LAPUJOULADE J., SALANON B., *Europhys. Lett.* **3** (1987) 737 ; FABRE F., GORSE D., SALANON B., LAPUJOULADE J., *Surf. Sci.* **175** (1986) L693.
[10] HELD G., JORDAN-SWEET J. L., HORN P. M., MAK A., BIRGENEAU R. J., *Phys. Rev. Lett.* **59** (1987) 2075.
[11] CHUI S. T., WEEKS J. D., *Phys. Rev. B* **14** (1976) 4978.
[12] VINEYARD G. H., *Phys. Rev. B* **26** (1982) 4146 ; DIETRICH S., WAGNER H., *Z. Phys.* B **56** (1984) 207.
[13] ROBINSON I. K., Handbook on Synchrotron Radiation, Eds. D. E. Moncton, G. S. Brown (North-Holland) vol. III (1989).
[14] ROBINSON I. K., MAC DOWELL A. A., ALTMAN M. S., ESTRUP P. J., EVANS-LUTTERODT K., BROCK J., BIRGENEAU R. J., *Phys. Rev. Lett.* **62** (1989) 1294.
[15] ROBINSON I. K., *Phys. Rev. B* **33** (1986) 3830.
[16] VAN BEIJEREN H., *Phys. Rev. Lett.* **38** (1977) 993.
[17] KNOPS H.J.F., *Ann. Phys. (N. Y.)* **128** (1980) 448.
[18] DEN NIJS M., RIEDEL E. K., CONRAD E. H., ENGEL T., *Phys. Rev. Lett.* **55** (1985) 1689.
[19] JOSE J. V., KADANOFF L. P., KIRKPATRICK S., NELSON D. R., *Phys. Rev. B* **16** (1969) 1217.
[20] FUOSS P. H., ROBINSON I. K., *Nucl. Inst. Meth.* **222** (1984) 171.
[21] PRAKASH J., HEMKAR M. P., *J. Phys. Soc. Jpn.* **36** (1974) 1608.
[22] CONRAD E. H., ALLEN L. R., BLANCHARD D. L., ENGEL T., *Surf. Sci.* **198** (1988) 207.
[23] FABRE F., SALANON B., LAPUJOULADE J., Structure of Surfaces II, Eds. J. F. van der Veen, M. A. van Hove (Springer, Berlin) 1988, p. 520.
[24] FABRE F., GORSE D., SALANON B., LAPUJOULADE J., *J. Phys. France* **48** (1987) 1017.
[25] DEN NIJS M., RIEDEL E. K., CONRAD E. H., ENGEL T., *Phys. Rev. Lett.* **57** (1986) 1279.
[26] MCKINNEY J. T., JONES E. R., WEBB M. B., *Phys. Rev. Suppl. 3* **160** (1967) 523.